RSC Advances

PAPER

View Article Online
View Journal | View Issue

Cite this: *RSC Adv.*, 2015, **5**, 17054

Sol–gel synthesis and room-temperature properties of α-$LiZr_2(PO_4)_3$†

Hany El-Shinawi,‡*[a] Colin Greaves[b] and Jürgen Janek[a]

Received 21st December 2014
Accepted 3rd February 2015

DOI: 10.1039/c4ra16804f

www.rsc.org/advances

The structural and electrical properties of α-$LiZr_2(PO_4)_3$ are studied at room temperature for the first time. A room-temperature stable α-$LiZr_2(PO_4)_3$ phase ($R\bar{3}c$, $a = 8.85196(4)$ Å and $c = 22.1510(1)$ Å) is prepared by a modified sol–gel approach. The material exhibits a room-temperature (25 °C) total conductivity of 1.63×10^{-6} Scm^{-1} at a density of 76% of the theoretical density. A room-temperature bulk conductivity as high as 1.58×10^{-4} Scm^{-1} can be estimated from the impedance measurements. Conductivity measurements suggest that a nominal α → α′ phase transition occurs below room-temperature (at about 16–18 °C). The activation energies for the conductivity of the α and α′ phases are 0.39 and 0.99 eV, respectively (in the temperature range −20 to 100 °C).

1. Introduction

Lithium ion conducting NASICONs are widely investigated as potential solid electrolytes for lithium battery applications. NASICON-structured $Li_xB_2(PO_4)_3$ phases exhibit a framework structure consisting of corner-shared PO_4 tetrahedra and BO_6 octahedra, which can accommodate lithium ions in two types of interstitial sites, commonly referred to as M1 and M2; the M1 sites are situated between pairs of BO_6 octahedra along the *c*-axis, while the M2 sites are located between infinite ribbons of $[O_3BO_3M1O_3BO_3\square O_3BO_3M1]\infty$ (Fig. 1). $LiB_2(PO_4)_3$ NASICONs ideally crystalize in the rhombohedral $R\bar{3}c$ space group where lithium selectively occupies the M1 sites. Among the different Li^+ conducting NASICONs, titanium-based ones exhibit the highest lithium ion conductivity at room temperature (up to 3×10^{-3} Scm^{-1} for $LiAl_{0.3}Ti_{1.7}(PO_4)_3$).[1,2] These solid electrolytes are, however, difficult to sinter and their grain boundary resistance is generally very high. A second disadvantage is the presence of Ti^{4+} which is easily reduced to Ti^{3+} in contact with low-potential anodes (Li metal or C_6Li) and also limits the use of the material as a solid separator in contact with aqueous electrolytes. $LiZr_2(PO_4)_3$, alternatively, is expected to be electrochemically more stable than the titanium analog since Zr^{4+} is a stable oxidation state in materials with related structure. However, $LiZr_2(PO_4)_3$ exhibits very low ionic conductivity at room-temperature ($\sim 10^{-8}$ Scm^{-1}).[3,4] The material also exhibits a complex polymorphism.[5–10] $LiZr_2(PO_4)_3$ phases prepared at relatively low calcination temperature (~900 °C), commonly denoted as β-type phases, are reported to be orthorhombic (β phase) above 300 °C and monoclinic (β′ phase: β-$Fe_2(SO_4)_3$-type structure) below this temperature.[7–9] $LiZr_2(PO_4)_3$ prepared at higher calcination temperatures (~1200 °C), on the other hand, is rhombohedral (α-$LiZr_2(PO_4)_3$) above a transition temperature varying in the range 30–60 °C; below this temperature, including room temperature, $LiZr_2(PO_4)_3$ is monoclinic/triclinic (α′-$LiZr_2(PO_4)_3$).[5–7,10–14] The ionic conductivity of α′-$LiZr_2(PO_4)_3$ is $\sim 5 \times 10^{-8}$ Scm^{-1} at 30 °C, while the conductivity of α-$LiZr_2(PO_4)_3$ at the same temperature is $\sim 10^{-5}$ Scm^{-1} as estimated from

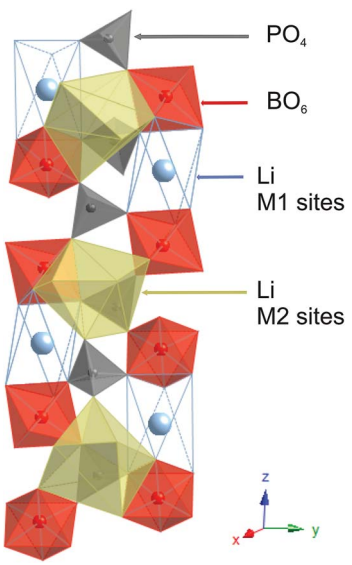

Fig. 1 Part of the NASICON-type crystal structure showing the M1 and M2 crystal sites.

[a]*Institute of Physical Chemistry, Justus-Liebig-University, Heinrich-Buff-Ring 58, 35392 Giessen, Germany. E-mail: H_elshinawi@mans.edu.eg; Fax: +49-641-99-34509; Tel: +49-641-99-34514*

[b]*School of Chemistry, University of Birmingham, Birmingham B15 2TT, UK*

† Electronic supplementary information (ESI) available. See DOI: 10.1039/c4ra16804f

‡ Permanent address: Chemistry department, Faculty of Science, Mansoura University, Mansoura 35516, Egypt.

extrapolating high-temperature measurements.[3,4] Efforts have therefore been directed to stabilize (rhombohedral) α-$LiZr_2(PO_4)_3$ at room temperature *via* several approaches such as varying synthesis conditions (*e.g.* quenching[15]) and aliovalent doping.[16–18] Mixed phases such as lithium zirconium/titanium phosphate and lithium zirconium phosphate/arsenate have also been prepared.[19,20] In this report a room-temperature stable α-$LiZr_2(PO_4)_3$ phase is successfully prepared using a modified sol–gel approach, which has enabled structural and electrical characterization of the material at room temperature for the first time.

2. Materials and methods

A modified sol–gel procedure was employed to synthesize $LiZr_2(PO_4)_3$. Lithium acetate (99.95%), zirconium oxynitrate hydrate (99%) and lithium dihydrogen phosphate (≥98.0%) were purchased from Aldrich and used as starting materials. The degree of hydration in zirconium oxynitrate was determined experimentally by thermogravimetric analysis. Stoichiometric amounts of lithium acetate and zirconium oxynitrate hydrate were first dissolved in hot dilute nitric acid solution (2–3 wt%) and then mixed slowly with EDTA (dissolved in NH_3 solution) and solid citric acid; mole ratio of total metal ions to EDTA and to citrate = 1 : 1 : 2. Dilute NH_3 solution was used to adjust the pH value of the solution to a value >7. After addition of drops of H_2O_2 solution (Aldrich, 30 wt%; H_2O_2/zirconium-ions mole ratio is greater than 1), a stoichiometric amount of lithium dihydrogen phosphate was then added slowly with continuous stirring. The resulting clear solution was heated at ~110 °C to produce a transparent gel, which was subsequently heated at 250 °C to form a black solid precursor. The solid precursor was ground and calcined in air at 550 °C for 24 h to remove organic components. The obtained powder was then isostatically pressed into pellets at 150 MPa and calcined in air at 1200 °C for 6 h. An alumina disc covered with a thick platinum sheet was used as a sample holder for the calcination step. The sintered pellets were then either crushed to be examined by X-ray powder diffraction (XRD) or directly used for conductivity measurements. We found that syntheses starting with ~5 wt% deficiency of the phosphate source (lithium dihydrogen phosphate) produce α-$LiZr_2(PO_4)_3$ phases of high purity.

X-ray diffraction (XRD) data were collected with an X'Pert Pro PANalytical (reflection mode) and a Bruker D8 (transmission mode) diffractometers, using CuKα radiations. Rietveld refinement based on XRD data were performed using the GSAS suite of programs.[21] Scanning electron microscopy (SEM) studies were performed using a MERLIN machine from Zeiss. AC impedance measurements were recorded using Alpha-A high performance modular measurement System (from Novocontrol technologies) in the frequency range of 10 MHz to 1 Hz and using an electrical perturbation of 20 mV. The data obtained were then analyzed by the software package WinDETA. Pellets with a thickness of 5–9 mm and a diameter of 10–13 mm were used in the conductivity measurements. Au electrodes were gas phase deposited on the circular sides of the pellets by thermal evaporation and copper discs were used to collect the current. Variable temperature conductivity measurements were carried out using a Novocool cryosystem (from Novocontrol technologies) in the temperature range −20 to 100 °C. Prior to each impedance measurement, the samples were equilibrated for 1 h at constant temperature. The differential scanning calorimetry (DSC) measurement was performed using a Seiko DSC 220 at a heating rate of 5 °C min^{-1}.

3. Results and discussion

XRD analysis of the as-prepared $LiZr_2(PO_4)_3$ showed that the material is single-phase with no evidence of impurity or unreacted phases (Fig. 2a). The XRD pattern of the material was readily indexed on a rhombohedral unit cell ($R\bar{3}c$ space group), consistent with a NASICON-type structure. The XRD pattern is characterized by the absence of the peak splitting which is commonly observed in previous studies and suggests a distortion of the NASICON-type structure.[8,15,22] No significant change is observed in the XRD pattern after storing the material for about one year (Fig. 2b; the inset), indicating that no relaxation of the framework from rhombohedral to monoclinic/triclinic has occurred. Rietveld refinement based on XRD data of $LiZr_2(PO_4)_3$ was performed using the GSAS suite of programs. The crystal structure was refined by starting from the ideal NASICON atomic coordinates with Zr, P and O atoms in the (12c), (18e) and (36f) Wyckoff positions, respectively, of the $R\bar{3}c$ space group. Li was assumed to occupy the M1 site [*i.e.* the (6b)

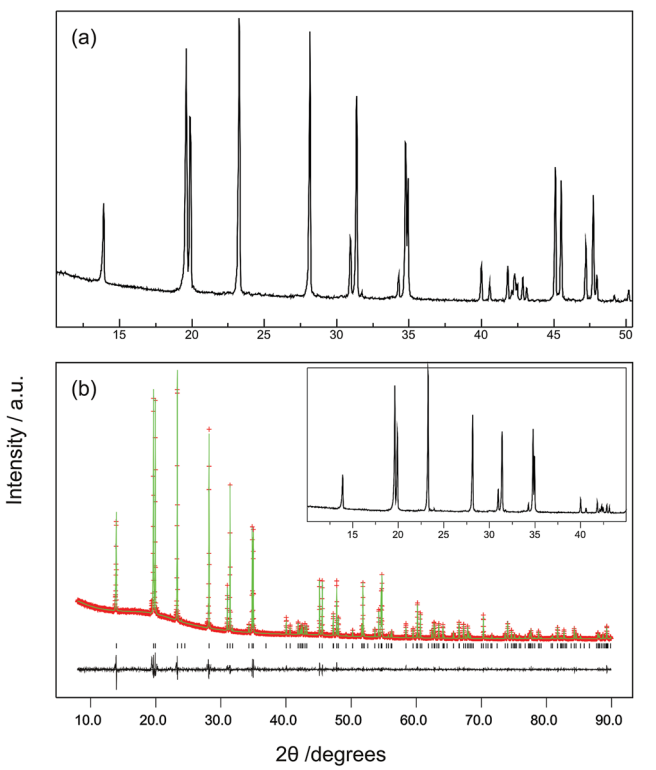

Fig. 2 (a) XRD pattern of as-prepared α-$LiZr_2(PO_4)_3$. (b) Observed (+), calculated and difference profiles (solid lines) for XRD data collected from α-$LiZr_2(PO_4)_3$ (λ = 1.5406 Å; wR_p = 0.0422, R_p = 0.0314, χ^2 = 2.103); the inset shows a part of the XRD pattern of α-$LiZr_2(PO_4)_3$ after storing the material for about one year.

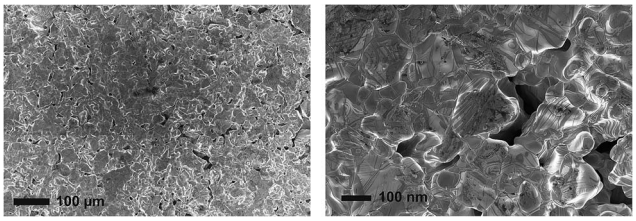

Fig. 3 Surface microstructure of a sintered pellet of α-$LiZr_2(PO_4)_3$.

position]. This refinement led to a good agreement between the experimental and calculated patterns (Fig. 2b) and to low reliability factors ($wR_p = 0.0422$, $R_p = 0.0314$, $\chi^2 = 2.103$). However, due to the low sensibility of the refinement to the occupancy of the Li ion sites, the suggested Li ion positions remain an assumption. The refined unit cell parameters are $a = 8.85196(4)$ Å and $c = 22.1510(1)$ Å. Interestingly, theses parameters are very close to those reported for α-$LiZr_2(PO_4)_3$ that is prepared by solid state reactions (at 1200 °C) and stabilized at 150 °C ($a = 8.85493(3)$ Å and $c = 22.1440(1)$ Å (ref. 13)). In earlier reports,[5,6] $LiZr_2(PO_4)_3$ is synthesized by the hydrolysis of an alcoholic solution containing zirconium alkoxide by using an aqueous solution containing lithium and phosphate ions; this procedure produces a monoclinic/triclinic $LiZr_2(PO_4)_3$ phase that converts to rhombohedral $LiZr_2(PO_4)_3$ (with $a \approx 8.85$ Å and $c \approx 22.24$ Å) above a transition temperature varying in the range 30–60 °C. Alamo *et al.* prepared $LiZr_2(PO_4)_3$ by dissolving reactants in acidic medium and claimed that the resulting phase is rhombohedral (with slight distortion) at room temperature, but they reported significantly different lattice parameters ($a \approx 8.79$ Å and $c \approx 22.78$ Å).[15,22] Hence, the α-$LiZr_2(PO_4)_3$ phase prepared in this study has similar lattice parameters to that stabilized at temperatures above room-temperature, indicating that the transition temperature of $LiZr_2(PO_4)_3$ has probably been lowered to a value below room temperature.

Similar to $LiTi_2(PO_4)_3$ and other NASICON-type phases, the as-prepared α-$LiZr_2(PO_4)_3$ phase showed low sinterability. The as-prepared pellets showed relatively low densities of about 74–77% of the theoretical densities. Fig. 3 shows the surface microstructure of the as-prepared α-$LiZr_2(PO_4)_3$ pellet. The grains are in good contact with each other although a large amount of pores can be observed.

The ionic conductivity of the as-prepared α-$LiZr_2(PO_4)_3$ was examined by AC impedance spectroscopy using gas-deposited gold electrodes. The impedance of the material shows a strong dependence on temperature. The impedance spectra can be described in terms of two semicircles (at high and intermediate frequencies) and a low frequency tail; and, over the studied frequency range, a shift of the observation window from left to right, *i.e.* towards lower frequencies, occurs as the temperature increases. Fig. 4 and S1 (ESI†) show the Nyquist impedance plots for the material (two different pellets) in a temperature range from −20 to 100 °C. The high frequency semicircle disappears from the spectra at temperatures >30 °C. However, this semicircle progressively appears, and the low frequency spike diminishes, as the temperature is decreased (Fig. 5). The impedance data were well fitted using $R(RQ)(Q)$, $R_e(RQ)(RQ)(Q)$ or $R_e(RQ)(RQ)$ equivalent circuits depending on

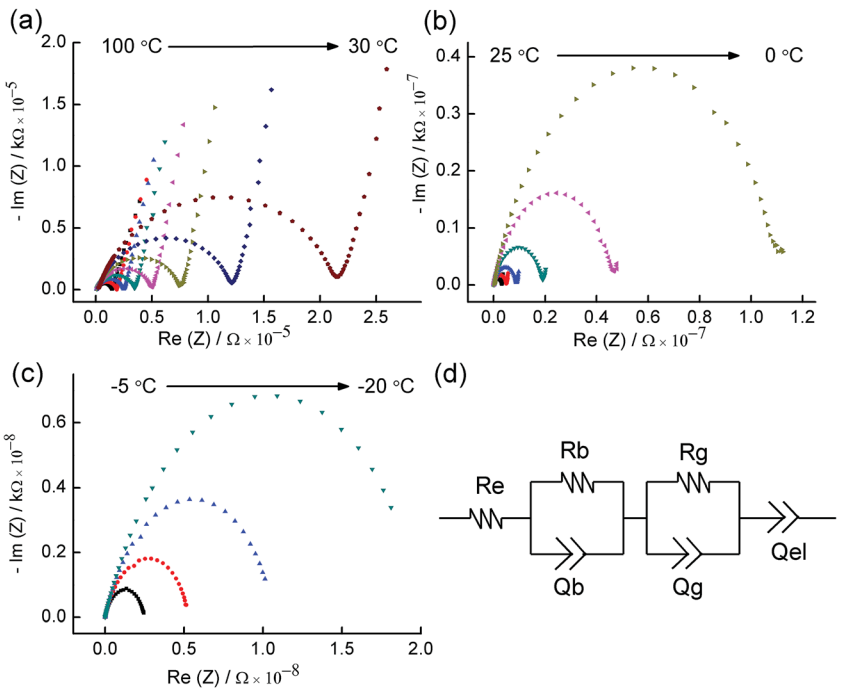

Fig. 4 (a–c) Impedance spectra for α-$LiZr_2(PO_4)_3$ measured using Au electrodes (frequency range from 10 MHz to 1 Hz; 20 mV amplitude) in the temperature range −20 to 100 °C. (d) An equivalent circuit of the type $R_e(RQ)(RQ)(Q)$; in the circuit, R is for resistance, Q for constant phase element and R_e for the electronic resistance of the measurement system; subscripts b, g and el refer to bulk, grain boundary and the blocking electrode, respectively.

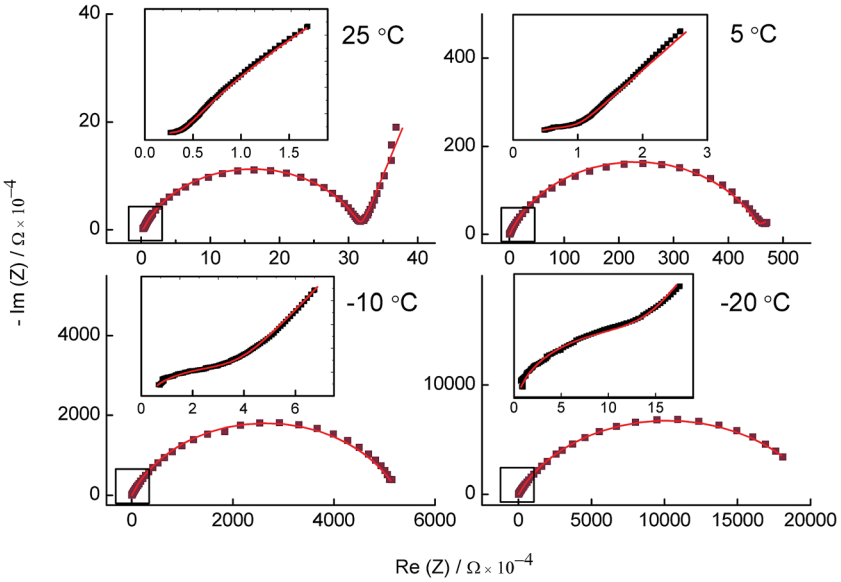

Fig. 5 Impedance spectra for α-$LiZr_2(PO_4)_3$ measured at 25, 5, −10 and −20 °C, and fitted using the equivalent circuit $R_e(RQ)(RQ)(Q)$ (25 °C) or $R_e(RQ)(RQ)$ (5, −10 and −20 °C). The insets show zoom views of the plots in the frequency range 10 MHz to 0.1 MHz.

the temperature; (*RQ*) [a parallel resistance/constant-phase-element] and (*Q*) [a constant phase element] correspond to a semicircle and the long tail in the *z* plane, respectively, while R_e is added to account for the electronic resistance of the measurement system. The impedance at 25 °C, for example, is fitted using the $R_e(RQ)(RQ)(Q)$ equivalent circuit (Fig. 4d). Although the high frequency semicircle is not fully defined in this plot (Fig. 5), the data were well fitted using $R_e(RQ)(RQ)(Q)$ rather than the $R(RQ)(Q)$ equivalent circuit. We generally attribute the first semicircle (high frequency), the second semicircle (intermediate frequency) and the low frequency tail to the impedance representing bulk, grain-boundary and electrode contributions, respectively. This is consistent with the results reported elsewhere where, within a fixed frequency range, the grain and grain boundary contributions to the impedance become more distinguishable, and the electrode contributions diminish, as the temperature decreases. This impedance behavior is also consistent with the behavior observed for isostructural $LiTi_2(PO_4)_3$.[23] For $LiTi_2(PO_4)_3$ (and using lithium borate as a sintering aid), the semicircles corresponding to bulk and grain-boundary effects were observed at −50 °C while both disappeared at 90 °C. Since Au blocking electrodes are used in our experiments, the appearance of the low frequency tail (at appropriate temperatures) generally suggests that the observed transport effect is mainly ionic and corresponds to lithium ion mobility.[24,25] The bulk conductivities of the material could be therefore estimated from the fitting data of the high frequency semicircle, or the intercept of the intermediate frequency semicircle (at the high frequency side) with the real *Z* axis (for data collected at temperatures >25 °C and fitted using $R(RQ)(Q)$ equivalent circuit).

The measured total and bulk conductivities of as-prepared α-$LiZr_2(PO_4)_3$ at room temperature (25 °C) are 1.63×10^{-6} and 1.58×10^{-4} Scm^{-1}, respectively. Another two different pellets showed total conductivities of 1.50×10^{-6} and 1.34×10^{-6} Scm^{-1}. These values are close to those reported for $LiTi_2(PO_4)_3$ (total conductivity 2.0×10^{-6} Scm^{-1}) which is isostructural to α-$LiZr_2(PO_4)_3$ and shows a similar morphology (lack of sinterability; ~34% porosity[2,26]). However, due to the absence of electrochemically active Ti^{4+}, a $LiZr_2(PO_4)_3$-based membrane probably shows better characteristics as a solid electrolyte in all-solid-state batteries or as a solid separator between different liquid electrolytes contacting the anode and cathode. Goodenough *et al.*[16] reported total and bulk conductivities of Ca-doped $LiZr_2(PO_4)_3$ as 4.9×10^{-5} Scm^{-1} and 1.2×10^{-4} Scm^{-1}, respectively. The bulk conductivity of $Li_{1.2}Zr_{1.9}Ca_{0.1}(PO_4)_3$ is similar to that observed for α-$LiZr_2(PO_4)_3$ in this study, however, the improved total conductivity is probably related to an improved sinterability due to Ca-doping. Hence, our study provides structural and conductivity data for α-$LiZr_2(PO_4)_3$ at room temperature that can be compared to the available data for isostructural phases such as $LiTi_2(PO_4)_3$, and also provide a base line for the ongoing attempts to stabilize and improve the sinterability of α-$LiZr_2(PO_4)_3$ by different approaches such as aliovalent doping.

The activation energy E_a for the Li-ion conduction of the material is obtained from the Arrhenius plot of $\sigma = \sigma_0 \exp(-E_a/kT)$, where σ_0 is the pre-exponential factor, k is the Boltzmann constant, T is the absolute temperature. The Arrhenius plots using the total and bulk ionic conductivities of α-$LiZr_2(PO_4)_3$ are shown in Fig. 6a and the corresponding inset, respectively. The plots clearly show an inflection point at 16–18 °C indicating a change in the Li ion mobility in the material. This is attributed to a phase transition from rhombohedral to monoclinic/triclinic $LiZr_2(PO_4)_3$. The observed activation energies for the total conductivity before and after the transition are 0.39 and 0.99 eV respectively. Boilot *et al.* reported a similar slope discontinuity in the conductivity data of

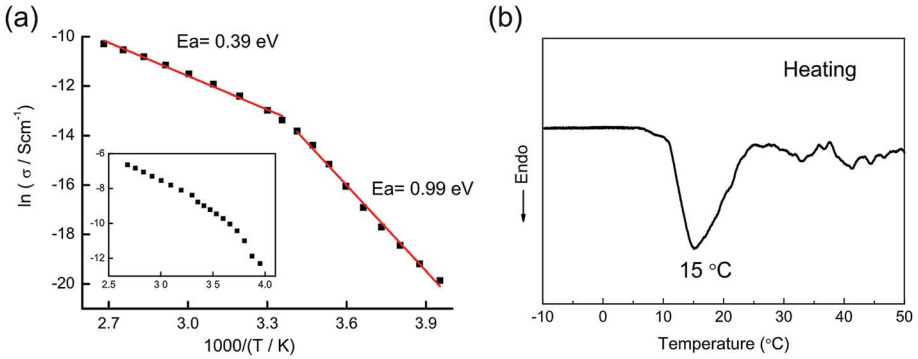

Fig. 6 (a) Arrhenius plots for the total and bulk (inset) ionic conductivities of α-$LiZr_2(PO_4)_3$. (b) The DSC curve of $LiZr_2(PO_4)_3$ recorded during a heating treatment.

$LiZr_2(PO_4)_3$ at ~40 °C with activation energies 0.42 and 0.65 eV before and after the transition, respectively; however, different temperature ranges were used in their study.[8] The observed activation energy in our study, in the temperature range ~20–100 °C, is slightly lower than that observed by Boilot *et al.* for $LiZr_2(PO_4)_3$ (ref. 8) and by Goodenough *et al.* for $Li_{1.2}Zr_{1.9}Ca_{0.1}(PO_4)_3$.[16,17] The variable-temperature conductivity data of $LiZr_2(PO_4)_3$ are consistent with the DSC data recorded from material in the temperature range −10 to 50 °C (Fig. 6b). An endothermic peak at ~15 °C is observed in the DSC curve of the material indicating that the as-prepared $LiZr_2(PO_4)_3$ exhibits $\alpha \rightarrow \alpha'$ transition below room temperature. Previous reports suggest that the $\alpha \rightarrow \alpha'$ transition in $LiZr_2(PO_4)_3$ occurs at temperatures varying in the range 30–60 °C depending on the synthetic method. The synthesis method employed in this study, however, suggests that this limit can be stretched so that the transition temperature lies below room temperature which enables structural and electrical characterization of the material at room temperature. Several structural modifications related to the synthesis method may have occurred and probably account for the room temperature stability of rhombohedral $LiZr_2(PO_4)_3$, *e.g.* a deficiency of phosphate groups, incorporation of traces of carbonate groups or a disturbance of the Li ion distribution in the NASICON structure. We have recently observed a synthesis-related disturbance of Li ion distribution in $LiTi_2(PO_4)_3$ that led to modified structural and electrochemical properties of the NASICON-type material.[27]

4. Conclusions

A modified sol–gel procedure that uses EDTA/citrate as complexing agent and employs a slight deficiency of the phosphate is successfully used to produce a room-temperature stable α-$LiZr_2(PO_4)_3$ phase. The as-prepared material undergoes no phase change upon storing for more than one year. The refined unit cell parameters are similar to those reported for α-$LiZr_2(PO_4)_3$ prepared by solid state reactions and stabilized at 150 °C. The measured total and bulk conductivities of as prepared α-$LiZr_2(PO_4)_3$ at room temperature (25 °C) are ~1.5×10^{-6} and 1.5×10^{-4} Scm^{-1}, respectively. The estimated bulk conductivity is comparable to those reported for $LiTi_2(PO_4)_3$ and $Li_{1.2}Zr_{1.9}Ca_{0.1}(PO_4)_3$. The material undergoes phase transition to the α′-phase below room temperature (at ~16–18 °C). The activation energies for the total conductivity before and after the transition are 0.39 and 0.99 eV, respectively (in a temperature range −20 to 100 °C).

Acknowledgements

The authors acknowledge support by the Humboldt foundation (H. E.-S.), the LOEWE project STORE-E and the LaMa (Laboratory of Materials Research) at Justus-Liebig University (State of Hessen).

References

1 H. Aono, E. Sugimoto, Y. Sadaoka, N. Imanaka and G. Y. Adachi, *J. Electrochem. Soc.*, 1989, **136**, 590–591.
2 H. Aono, E. Sugimoto, Y. Sadaoka, N. Imanaka and G. Adachi, *J. Electrochem. Soc.*, 1990, **137**, 1023–1027.
3 J. Kuwano, N. Sato, M. Kato and K. Takano, *Solid State Ionics*, 1994, **70**, 332–336.
4 K. Nomura, S. Ikeda, K. Ito and H. Einaga, *Solid State Ionics*, 1993, **61**, 293–301.
5 D. Petit, P. Colomban, G. Collin and J. P. Boilot, *Mater. Res. Bull.*, 1986, **21**, 365–371.
6 D. Petit and B. Sapoval, *Solid State Ionics*, 1986, **21**, 293–304.
7 M. Casciola, U. Costantino, L. Merlini, I. G. Krogh Andersen and E. Krogh Andersen, *Solid State Ionics*, 1988, **26**, 229–235.
8 F. Sudreau, D. Petit and J. P. Boilot, *J. Solid State Chem.*, 1989, **83**, 78–90.
9 M. Catti, N. Morgante and R. M. Ibberson, *J. Solid State Chem.*, 2000, **152**, 340–347.
10 K. Arbi, M. Ayadi-Trabelsi and J. Sanz, *J. Mater. Chem.*, 2002, **12**, 2985–2990.
11 J. E. Iglesias and C. Pecharromán, *Solid State Ionics*, 1998, **112**, 309–318.
12 M. Catti, S. Stramare and R. Ibberson, *Solid State Ionics*, 1999, **123**, 173–180.
13 M. Catti and S. Stramare, *Solid State Ionics*, 2000, **136**, 489–494.

14 M. Catti, A. Comotti and S. Di Blas, *Chem. Mater.*, 2003, **15**, 1628–1632.
15 J. Sanz, J. M. Rojo, R. Jiménez, J. E. Iglesias and J. Alamo, *Solid State Ionics*, 1993, **62**, 287–292.
16 H. Xie, J. B. Goodenough and Y. Li, *J. Power Sources*, 2011, **196**, 7760–7762.
17 H. Xie, Y. Li and J. B. Goodenough, *RSC Adv.*, 2011, **1**, 1728–1731.
18 Y. Li, M. Liu, K. Liu and C.-A. Wang, *J. Power Sources*, 2013, **240**, 50–53.
19 A. Venkateswara Rao, V. Veeraiah, A. V. Prasada Rao, B. Kishore Babu and K. Vijaya Kumar, *Ceram. Int.*, 2014, **40**, 13911–13916.
20 V. I. Petkov, M. V. Sukhanov, A. S. Shipilov, V. S. Kurazhkovskaya, E. Y. Borovikova, I. Y. Pinus and A. B. Yaroslavtsev, *Inorg. Mater.*, 2014, **50**, 263–272.
21 A. C. Larson and R. B. Von Dreele, *General Structural Analysis System*, Los Alamos National Laboratory, Los Alamos, NM, 1994.
22 J. Alamo and J. L. Rodrigo, *Solid State Ionics*, 1989, **32**, 70–76.
23 H. Aono, E. Sugimoto, Y. Sadaoka, N. Imanaka and G.-y. Adachi, *Solid State Ionics*, 1991, **47**, 257–264.
24 V. Thangadurai, R. A. Huggins and W. Weppner, *J. Power Sources*, 2002, **108**, 64–69.
25 J. T. S. Irvine, D. C. Sinclair and A. R. West, *Adv. Mater.*, 1990, **2**, 132–138.
26 G.-y. Adachi, N. Imanaka and H. Aono, *Adv. Mater.*, 1996, **8**, 127–135.
27 H. El-Shinawi and J. Janek, *RSC Adv.*, 2015, **5**, 14887–14891.